ITG-like Instability in the Two-fluid Model in Slab Geometry

D. D. Schnack[*], D. C. Barnes[†], Ping Zhu, C. C. Hegna and C. R. Sovinec

Center for Plasma Theory and Computation

Department of Engineering Physics

University of Wisconsin - Madison

Madison, WI 53706

December 21, 2011

Abstract

We attempt to verify the NIMROD code by direct comparison with analytic solutions for the case of a plasma with uniform equilibrium density and electron temperature, but with a gradient of the equilibrium ion temperature, in Cartesian slab geometry. Local analytic solutions of the two-fluid equations are developed. It is found that the system is unstable if the gyro-viscous stress is included, but the results to not agree with the predictions of kinetic theory. Agreement requires that the ion diamagnetic heat flux also be included in the model. Presently, the NIMROD code has implemented the full gyro-viscous stress tensor, but the model for diamagnetic heat flux is still undergoing testing and debugging. Therefore, NIMROD solutions can only be compared with the analytic model that ignores the diamagnetic heat flux. Good agreement is found between these analytic and computational solutions. However, the model is incomplete and neither solution agrees with the results of kinetic theory. Therefore, NIMROD has been verified but not validated by this exercise. More physically realistic tests require completion of the implementation of the diamagnetic heat flux in NIMROD.

[*]Department of Physics
[†]TriAlpha Corp.

1

1 Introduction

The ion temperature gradient mode, or ITG, is a parallel sound wave that becomes unstable in the presence of an ion temperature gradient and relative drifts between the ions and the electrons. It was first derived from kinetic theory [1, 2], and also from the moment, or fluid, equations by several authors, [2, 3, 4]. It has been reviewed in the context of a cause of anomalous transport in tokamaks [5], and it has become a textbook problem in kinetic theory [6].

The ITG is most virulent in regions where the equilibrium plasma density is almost spatially uniform and the ion pressure is almost all due to the equilibrium ion temperature gradient. With slab geometry, a uniform magnetic field B_0 in the z-direction, a static electric field, and constant density and electron temperature, this theory leads to an approximate cubic dispersion relation of the form

$$\left(\omega^2 - \omega_{s*}^2\right)\omega - \omega_{se}^2\omega_{*Ti} = 0 \; , \tag{1}$$

where $\omega_{s*} = k_z C_{s*}$ is the total parallel hybrid sound frequency (using the ion and electron temperatures and the ion mass), $\omega_{se} = k_z C_{se}$ is the parallel electron sound frequency, and $\omega_{*Ti} = (k_y/eB_0)dT_{i0}/dx$, which has the form of the perpendicular ion drift velocity, but enters the theory in completely different way [3]. When $\omega_{*Ti} << (C_s^2/C_*^2)\omega$, the balance between the cubic and linear terms leads to a stable parallel sound wave. When $\omega_{s*}^2 << \omega^2 << (C_*^2/C_{s*}^2)\omega_{*Ti}^2$, the balance is between the cubic term and the linear term. Then

$$\omega^3 = \frac{k_y k_z^2 T_{e0}}{eB_0 M}\frac{dT_{i0}}{dx} \; , \tag{2}$$

which has three roots $\omega_n = |A|^{1/3}e^{2\pi in/3}, n = 0, 1, 2$, and ω_2 has a negative imaginary part. This is the growth rate γ of the ITG; the real part of ω_2 gives the real frequency of the mode. It is customary to write $dT_{i0}/dx \sim \eta_i T_{i0}$, so that $\gamma \sim \eta_i^{1/3}$. The ITG is also called the "η_i mode". "The [last] term in [Equation (1)] represents an additional pumping of temperature in the ion waves due to transversal [sic] transport of heat in a nonuniform plasma ... The unstable root corresponds to the possibility of always having the additional pumping ... in phase with the growing temperature for the ion sound waves"[2].

The ITG mode is stable with the context of ideal, resistive, and Hall MHD. Instability requires finite Larmor radius (FLR) effects. In contrast, interchange-like modes (e.g., the g-mode) are ideal MHD modes that are stabilized by two-fluid (i.e., Hall) and FLR effects in slab geometry.

1.1 The Extended MHD Model

In terms of non-dimensional variables, the extended MHD equations are

$$\frac{\partial n}{\partial t} = -\nabla \cdot (n\mathbf{V}) \ , \tag{3}$$

$$Mn\frac{d\mathbf{V}}{dt} = \mathbf{J} \times \mathbf{B} - \frac{1}{2}\beta\nabla p - \frac{1}{2}\beta_i \delta_i \nabla \cdot \mathbf{\Pi}^{gv} \ , \tag{4}$$

$$\frac{\partial \mathbf{B}}{\partial t} = -\nabla \times \mathbf{E} \ , \tag{5}$$

$$\mathbf{E} = -\mathbf{V} \times \mathbf{B} + \frac{1}{n}\delta_i \left(\mathbf{J} \times \mathbf{B} - \frac{1}{2}\beta_e \nabla p_e\right) \ , \tag{6}$$

$$\frac{dp_i}{dt} = -\Gamma_i p_i \nabla \cdot \mathbf{V} - (\Gamma_i - 1)\frac{1}{2}\beta_i \delta_i \nabla \cdot \mathbf{q}^i_{gv} \ , \tag{7}$$

and

$$\frac{dp_e}{dt} = -\Gamma_e p_e \nabla \cdot \mathbf{V}_e \ , \tag{8}$$

where $d/dt = \partial/\partial t + \mathbf{V} \cdot \nabla\mathbf{V}$ is the advective derivative. Length is measured in terms of a characteristic system size a, density is measured in terms of a characteristic (or mean) density n_0, the magnetic field in terms of the characteristic value B_0, and the species pressure is measured in terms of the characteristic pressure p_{s0}, $s = e, i$. The equation of state for each species is $p_s = nT_s$. The species velocity is measured in units of the Alfvén speed $V_A = B_0/\sqrt{\mu_0 n_0 M}$, and time in units of $t_0 = a/V_A$, so that frequency is measured in units of $\omega_A = 1/t_0 = V_A/a$. The total pressure is $p = p_i + p_e$, $\beta_s \equiv 2\mu_0 p_{s0}/B_0^2$, $\beta = \beta_e + \beta_i$, and $\delta_i \equiv d_i/a = c/(\omega_{pi}a)$. Current density is measured in units of $B_0/(\mu_0 a)$, so that $\mathbf{J} = \nabla \times \mathbf{B}$ and $\delta_i \mathbf{J} = n(\mathbf{V} - \mathbf{V}_e)$. In general, $\mathbf{V}$ is the center of mass velocity, but in this form $m_e = 0$, so $\mathbf{V}$ is the (non-dimensional) ion velocity. The electron velocity $\mathbf{V}_e = \mathbf{V} - \delta_i \mathbf{J}/n$ is used in Equation (8), including the advective derivative of p_e.

The non-dimensional gyro-viscous stress tensor is

$$\mathbf{\Pi}^{gv} = \frac{\eta_3}{2}\left[\hat{\mathbf{b}} \times \mathsf{W} \cdot \left(\mathsf{I} + 3\hat{\mathbf{b}}\hat{\mathbf{b}}\right) + \text{transpose}\right] \equiv \frac{\eta_3}{2}\mathsf{F} \cdot \mathsf{W}(\mathbf{V}) \ , \tag{9}$$

where F is a tensor operator of rank four (the elastic constant tensor), $\eta_3 = p_i/2B$, $\hat{\mathbf{b}} = \mathbf{B}/B$, and

$$\mathsf{W}_{i,j}(\mathbf{V}) = \frac{\partial V_j}{\partial x_i} + \frac{\partial V_i}{\partial x_j} - \frac{2}{3}\delta_{i,j}\nabla \cdot \mathbf{V} \ , \tag{10}$$

is the rate of strain tensor. The ion diamagnetic heat flux is

$$\mathbf{q}^i_{gv} = \kappa^i_{gv}\hat{\mathbf{b}} \times \nabla T_i \ . \tag{11}$$

3

where $\kappa_{gv}^i = (5/2)(p_i/B)$. In unsheared slab geometry, the divergence of Eq. (11) can be written as

$$\nabla \cdot \mathbf{q}_{gv}^i = \frac{5}{2}\frac{1}{B_0}\hat{\mathbf{b}} \cdot (\nabla T_i \times \nabla p_i), \tag{12}$$

$$= \frac{5}{2}\frac{T_i}{nB_0}\hat{\mathbf{b}} \cdot (\nabla p_i \times \nabla n). \tag{13}$$

The parameters Γ_i and Γ_e are the "adiabatic" contants for the ions and electrons. Since the characteristic time scale for the ITG is assumed to be long compared with $1/\Omega$, it is customary to assume that the electrons are isothermal, i.e., $\Gamma_e = 1$. However, direct comparison between the theory and the computations require $\Gamma_e = 5/3$. We always take $\Gamma_i = 5/3$.

Equations (9 - 13) describe to lowest order the collisionless "transport" arising from the small but finite ion Larmor radius; they represent a non-dissipative transport of momentum and energy due to the spatial variation of the magnetic moments of the gyrating ions[11]. Since this "transport" is not a result of particle collisions, its effects are completely reversible. Equations (3 - 8) reduce to ideal MHD in the limit $\delta_i \to 0$.

Various forms of Equations (3 - 8) are now commonly used in linear and nonlinear numerical simulation of tokamak plasmas [8, 9]. An important step in the verification of these computational models is to test their ability to detect accurately instabilities such as the ITG that depend intrinsically on two-fluid and FLR effects.

The specific computational model used in this work [8] solves the "primitive" form [10] of Equations (3 - 8) in specified geometry without further assumptions. Verification of these computational results requires direct comparison with the predictions of a theory that makes the minimum number of assumptions. Nonetheless, the complexity of the mathematics involved in solving the analytic model still dictates a number of simplifying assumptions. In particular, the equilibrium in slab geometry has a unidirectional magnetic field $\mathbf{B}(x) = B_0(x)\hat{\mathbf{e}}_z$ that varies only in the x-direction. Perturbations to the equilibrium are assumed to vary as $f = \hat{f}e^{i(\omega t + k_y y + k_z z)}$, where $\hat{f}$ is independent of x. This "local approximation" reduces the problem to algebra. (However, x-derivatives of equilibrium quantities must be included.) Further, since for fusion applications we are primarily interested in frequencies that are comparable with or less than the Alfvén frequency $\omega_A = V_A/a$ and parallel wavelengths that are much longer than perpendicular wavelengths, we can introduce a small parameter $k_z/k_y \sim \epsilon^2 << 1$, and assume $\omega/\omega_A \leq 1$. This "ballooning ordering" further simplifies the algebra, but in most cases we can obtain a dispersion relation only to lowest order in ϵ. We also take $T_{e0} = $ constant and $n_0 = $ constant.

4

1.2 FLR Cancellations

The collisionless, reversible "transport" embodied in the ion gyro-viscous stress, Equation (9), and the ion diamagnetic heat flux heat flux, Equation (11), represent the lowest order (in $k_\perp \rho_i$) effects of finite ion Larmor radius (FLR) when $\beta_i > 0$. These terms cancel, either whole or in part, the terms describing advection by the ion diamagnetic drift velocity $\mathbf{V}_{*i} \cdot \nabla$. This has a significant effect on the stability properties of the extended MHD model.

The first of these occurs within the ion momentum equation, and can be written, in SI units, as $Mn\mathbf{V}_{*i} \cdot \nabla\mathbf{V} + \nabla \cdot \mathbf{\Pi}_i^{gv} \approx 0$. This is called the *gyro-viscous cancellation*, because it involves the ion gyro-viscous force. This is motivated by the form of the gyro-viscous stress, Equation (9); in cartesian coordinates, the relevant terms of the x-component of the ion momentum equation are (in SI units)

$$i\left(\omega + \frac{k_y}{n_0 e B_0}\frac{dp_{i0}}{dx}\right) V_x = -\frac{1}{Mn_0}\frac{\partial \Pi_{xx}^{gv}}{\partial x} \approx \frac{ik_y V_x}{2n_0 e B_0}\frac{dp_{i0}}{dx} + \dots \;. \qquad (14)$$

The gyro-viscous force therefore cancels at least part ($\sim 1/2$) of the advection from the diamagnetic drift. In analytic work the cancellation is often assumed to be complete, i.e., $Mn\mathbf{V}_{*i} \cdot \nabla\mathbf{V}_i + \cdot\mathbf{\Pi}_i^{gv} = 0$. This assumption greatly simplifies both the equations and the ensuing algebra (see Ref. [11] for a more thorough discussion). Clearly the situation is more complicated.

The second cancellation, arising from the ion diamagnetic heat flux, involves the ion energy equation, Equation (7), and the ion continuity equation, Equation (18): $(3/2)\nabla \cdot \mathbf{q}_i^{gv}$ cancels the advection of density by the ion diamagnetic drift $\mathbf{V}_{*i} \cdot \nabla n$. This can be seen as follows.

Decompose the (nonlinear) velocity as $\mathbf{V} = \mathbf{V}_i + \mathbf{V}_{*i}$, where $\mathbf{V}_{*i} = \hat{\mathbf{b}} \times \nabla p_i/(neB)$ is the diamagnetic drift velocity. The velocity $\mathbf{V}_i$ contains all the dynamical parts of the ion flow plus the $E \times B$ drift. Solve Equation (18) for $\nabla \cdot \mathbf{V}_i$ (using $\nabla \cdot \mathbf{V}_{*i} = 0$), and substitute this expression into Equation (7). The result is

$$\begin{aligned}
\frac{\partial p_i}{\partial t} + (\mathbf{V}_i + \mathbf{V}_{*i}) \cdot \nabla p_i &= \frac{5}{3}\frac{p_i}{n}\frac{\partial n}{\partial t} + \frac{5}{3}\frac{p_i}{n}\mathbf{V}_i \cdot \nabla n \\
&\quad + \frac{5}{3}\frac{p_i}{n}\mathbf{V}_{*i} \cdot \nabla n - \frac{2}{3}\nabla \cdot \mathbf{q}_i^{gv}.
\end{aligned} \qquad (15)$$

We concentrate on the last two terms on the right hand side. From the definition of $\mathbf{V}_{*i}$ and $p_i = nT_i$, we have

$$\begin{aligned}
\mathbf{V}_{*i} \cdot \nabla n &= \frac{1}{neB}\hat{\mathbf{b}} \times \nabla p_i \cdot \nabla n \\
&= \frac{1}{eB}\hat{\mathbf{b}} \cdot (\nabla T_i \times \nabla n).
\end{aligned} \qquad (16)$$

Then using Equation (12),

$$
\begin{aligned}
\frac{5}{3}\frac{p_i}{n}\mathbf{V}_{*i} \cdot \nabla n - \frac{2}{3}\nabla \cdot \mathbf{q}_i^{gv} \;=\;& \frac{5}{3}\frac{T_i}{eB}\hat{\mathbf{b}} \cdot (\nabla T_i \times \nabla n) \\
& - \left(\frac{2}{3}\right)\left(\frac{5}{2}\right)\frac{T_i}{eB}\hat{\mathbf{b}} \cdot (\nabla T_i \times \nabla n) \\
\;=\;& 0. \qquad\qquad\qquad (17)
\end{aligned}
$$

Unlike the gyro-viscous cancellation, this cancellation is complete (i.e., exact) for electrostatic modes in unsheared slab geometry where $\nabla \times \hat{\mathbf{b}}_0 = 0$; in the more general case the right hand side is $-(2/3)(p_i/eB)\nabla T_i \cdot \nabla \times \hat{\mathbf{b}}$. To our knowledge, this cancellation has no special name in the literature, although it is widely used. For lack of a better term, we refer to it as the *diamagnetic heat cancellation.*

We shall see that both the gyro-viscous cancellation and the diamagnetic heat flux cancellation must be included in the two-fluid model to obtain results consistent with kinetic theory, where they arise naturally.

2 Analytical Model

The theory of the ITG is well-known [1, 2], and has been extended to include the effects of magnetic shear and toroidal geometry [12, 13]. Computational results for the ITG have used gyro-fluid models [14] and gyro-kinetic models [15]. To the best of our knowledge, ITG-like modes have not been previously calculated with an extended MHD model. In order to verify the computational results, it is desirable to have an appropriate analytic solution of these equations. Ideally, this theory would provide an exact solution of the same equations as solved in the computational algorithm. This is impractical, if for no other reason that the resulting analytic model would be a set of differential equations that would need to be solved numerically. Here we attempt to find an approximate analytical solution of the extended MHD equations, or their equivalent set of two-fluid equations, that requires as few assumptions as possible while retaining algebraic tractability. We emphasize that we do not intend to present a new theory of the ITG; rather, we find approximate solutions of the extended MHD equations (i.e., the equivalent two-fluid equations) that are as close as practical to those solved in the computational model, and compare them with the numerical solutions.

For the analysis, we use a two-fluid model in which the ions and electrons have individual velocities, temperatures, and pressures, and obey separate continuity, momentum and energy equations. Assuming quasi-neutrality, so that $n_i = n_e = n$, neglecting the electron mass ($m_e = 0$), and using the same normalization as in

Equations (3)-(8), these equations are ion continuity,

$$\frac{\partial n}{\partial t} = -\nabla\left(n\mathbf{V}_i\right) \ , \tag{18}$$

electron continuity,

$$\frac{\partial n}{\partial t} = -\nabla\left(n\mathbf{V}_e\right) \ , \tag{19}$$

ion momentum,

$$\delta_i n \frac{d\mathbf{V}_i}{dt} = n\left(\mathbf{E} + \mathbf{V}_i \times \mathbf{B}\right) - \frac{1}{2}\beta_i\delta_i\left(\nabla p_i - \delta_i\nabla\cdot\mathbf{\Pi}_i^{gv}\right), \tag{20}$$

and electron momentum,

$$0 = -n(\mathbf{E} + \mathbf{V}_e \times \mathbf{B}) - \frac{1}{2}\beta_e\delta_i\nabla p_e \ , \tag{21}$$

along with Equations (7) (with $\mathbf{V} = \mathbf{V}_i$) and (8). The electric field is

$$\mathbf{E} = \mathbf{E}_0 - \nabla\phi - \frac{\partial\mathbf{A}}{\partial t} \ , \tag{22}$$

where $\mathbf{E}_0$ is a constant externally applied field, $\mathbf{A}$ is the vector potential, $\mathbf{B} = \nabla \times \mathbf{A}$, and ϕ is the scalar potential. (Here, $\mathbf{E}$ is measured in units of $V_A B_0$, ϕ is measured in units of $\phi_0 = \Omega a^2 B_0$ and $\mathbf{A}$ is measured in units of $A_0 = B_0 a = E_0 t_0$.) These must be supplemented by Ampére's law, Equation (5), and Faraday's law

$$\delta_i\mathbf{J} = n\left(\mathbf{V}_i - \mathbf{V}_e\right), \tag{23}$$
$$= \delta_i\nabla \times \mathbf{B}. \tag{24}$$

These equations are equivalent to the extended MHD equations, Equations (3-8). Identifying $\mathbf{V} = \mathbf{V}_i$, Equation (18) becomes Equation (3); subtracting Equations (18) and (19) yields $\nabla\cdot\mathbf{J} = 0$, consistent with Equations (23) and (24). Adding Equations (20) and (21) eliminates $\mathbf{E}$ and, using Equation(23), and dividing out a common factor of δ_i, yields Equation (4), while using Equation (23) in Equation (21) yields the extended Ohm's law, Equation (6). (These manipulations also require the electron pressure to be expressed in the ion frame of reference; we omit the details. Further, the required division by δ_i precludes setting $\delta_i = 0$; ideal MHD is obtained directly from Equations (18) - (24) only in the *limit* $\delta_i \to 0$.)

The equation for the electromagnetic field is found by introducing $\mathbf{B} = \nabla \times \mathbf{A}$ into Equation (24), using Equation (23), and imposing the gauge condition $\nabla\cdot\mathbf{A} = 0$:

$$\delta_i\nabla^2\mathbf{A} = -n\left(\mathbf{V}_i - \mathbf{V}_e\right) \ . \tag{25}$$

This couples the ion and electron dynamics.

We will determine the stability of the system by considering the evolution of small perturbations about a steady equilibrium (force balance) state. We work in simple slab geometry (x, y, z), where equilibrium quantities can vary in x; y and z are periodic coordinates. (In the computations, there are perfectly conducting walls at $x = \pm a$.) We will denote equilibrium quantities by the subscript $(\ldots)_0$. The equilibrium is characterized by $\partial/\partial t = 0$ but $\mathbf{V}_{s0} \neq 0$. The magnetic field is $\mathbf{B}_0 = B_0(x)\hat{\mathbf{e}}_z$. The condition for force balance is

$$\frac{d}{dx}\left[B_0(x)^2 + \beta_i p_{i0}(x) + \beta_e p_{e0}(x) \right] = 0 \ , \tag{26}$$

where $B_0(0) = p_{i0}(0) = p_{e0}(0) = 1$. The remaining equilibrium conditions are given by the ion and electron drift velocities

$$V_{sy0}(x) = -\frac{E_{x0}}{B_0(x)} \pm \frac{1}{2}\frac{\beta_s \delta_i}{B_0(x)}\frac{dp_{s0}(x)}{dx} \ , \tag{27}$$

where the $(+)$ sign is for ions, the $(-)$ sign is for electons, $p_{s0}(x) = n_0(x)T_{s0}(x)$, and E_{x0} is a constant applied electric field whose value can be chosen arbitrarily (and for convenience), and determines the frame of reference.

In this work we chose the particular functional dependence $n_0 = $ constant, $T_{e0}(x) = 1$, and $T_{i0}(x) = e^{\eta_i x}$, where $\eta_i \equiv a/L_{Ti}$, and L_{Ti} is the scale length for variations in the ion temperature. Then

$$B_0(x) = \sqrt{1 - \beta_i \left[e^{\eta_i x} - 1 \right]} \ , \tag{28}$$

$$V_{iy0}(x) = -\frac{E_{x0}}{B_0(x)} + \frac{\beta_i \delta_i \eta_i}{2B_0(x)}e^{\eta_i x} \ , \tag{29}$$

and

$$V_{ey0}(x) = -\frac{E_{x0}}{B_0(x)} \ . \tag{30}$$

From Equation (29), $E_{x0} \sim O(\delta_i)$, and we will sometimes write $E_{x0} = \mathcal{E}_{x0}\delta_i$. This equilibrium is stable in ideal MHD.

We note that Equation (28) requires that

$$\eta_i < \ln\left(\frac{1 + \beta_i}{\beta_i}\right) \ . \tag{31}$$

The linearized non-dimensional two-fluid equations are elucidated in Appendix A. These comprise sixteen equations in the sixteen unknowns n (1), $\mathbf{V}_i$ (3), $\mathbf{V}_e$ (3), ϕ (1), p_i (1), p_e (1), $\mathbf{A}$ (3), and $\mathbf{B}$ (3). These [i.e., Equations (53) - (60) of Appendix

A] are differential equations, and are the equations solved in the computational model [8]. They can be reduced to an algebraic system of equations by assuming the perturbed quantities vary as $f = \hat{f}e^{i(wt+\alpha_y y+\alpha_z z)}$, where $w = \omega/\omega_A$ is the non-dimensional frequency, $\alpha_y = k_y a$ and $\alpha_z = k_z a$ are non-dimensional wave numbers, $\hat{f}$ is assumed to be independent of x, accounting for the x-dependence of the equilibrium quantities, and evaluating the resulting expressions at $x = 0$.

Most analytical studies of two-fluid instabilities such as the ITG proceed by algebraic manipulation of the individual equations of the model, with appropriate approximations made at crucial points in the calculation. In this work we retreat behind formalism. The individual algebraic equations, with isothermal electrons ($\Gamma_e = 1$) are elucidated in Appendix B. These are a homogeneous algebraic system in the unknowns $(n, V_{xi}, V_{yi}, V_{zi}, V_{xe}, V_{ye}, V_{ze}, p_i, p_e, \phi, A_x, A_y, A_z, B_x, B_y, B_z)$. Non-trivial solutions require that the determinant of the system vanish. This yields an eighth order algebraic equation $F(w) = 0$ for the non-dimensional frequency w; there are eight roots. The system is stable if all the roots are real.

The equation $F(w) = 0$ can be solved without further approximation in some simple cases. When $\eta_i = 0$ (a uniform medium), $\beta_i = \beta_e = 0$, and $\alpha_y = 0$, $F(w) = 0$ is a quadratic equation in w^2. There are no FLR effects. When $\alpha_z = 0$, the roots are $w_\pm^2 = \alpha_y^2$, which are compressional Alfvén waves. When $\alpha_y = 0$, the roots are

$$w_\pm^2 = \alpha_z^2 \left(1 + \frac{1}{2}\alpha_z^2\delta_i^2 \pm \alpha_z\delta_i\sqrt{1 + \frac{1}{4}\alpha_z^2\delta_i^2}\right) \ . \tag{32}$$

The first term is the shear Alfvén wave, the second term is the whistler wave, and the last terms are two fluid corrections ($\sim \alpha_z\delta_i = k_z d_i$). At finite β, when $\alpha_y = 0$ the roots are the usual parallel sound waves $w_\pm^2 = (2/3)\alpha_z^2$, and four more complicated roots that contain two fluid and FLR corrections. When $\alpha_z = 0$, the roots are

$$w_\pm^2 = \alpha_y^2 \left(1 + \frac{2}{3}\beta + \frac{1}{64}\alpha_y^2\beta^2\delta_i^2\right) \ . \tag{33}$$

The first two terms are magneto-acoustic waves, and the last term is an FLR correction ($\sim \alpha_y\beta\delta_i = k_y\rho_i$), where $\rho_i = V_{thi}/\Omega$ is the ion gyro-radius.

For other situations the solvability condition is more complicated. We are interested in solutions corresponding to long parallel wavelength, short perpendicular wavelength, and relatively low frequency, on the order of ω_A or less. We therefore introduce a small parameter $\epsilon << 1$, and order $\alpha_y \sim 1/\epsilon^2 >> 1$, $\alpha_z \sim 1$, and $w \sim 1$. We also order $E_{x0} \sim \epsilon^2$ and $\delta_i \sim \epsilon^2$. All other parameters are $O(1)$ or less. Then the solvability condition contains only even powers of ϵ, and can be written as

$$F(w) = F_0(w) + F_2(w)\epsilon^2 + F_4(w)\epsilon^4 + \dots \ , \tag{34}$$

9

so that, to lowest order in ϵ, the solvability condition is $F_0(w) = 0$. This is generally a simpler equation (i.e., lower order in w) than $F(w) = 0$, and possibly easier to solve.

2.1 Electrostatic Modes

2.1.1 The Cubic Dispersion Relation

We first consider the electrostatic case, $\mathbf{E} = -\nabla\phi$. Then $F_0(w) = 0$ is a quartic equation in w, which factors as

$$w = \mathcal{E}_{x0}\delta_i\alpha_y \ , \tag{35}$$

times a cubic $f_3(w) = 0$ of the form

$$a_3 w^3 + a_2 w^2 + a_1 w + a_0 = 0 \ . \tag{36}$$

Equation (35) depends explicitly on the equilibrium electric field (the frame of reference) and vanishes when $\mathcal{E}_{x0} = 0$; it is just the zero frequency mode $\omega - k_y V_E = 0$ in the Doppler shifted reference frame. In Equation (36), the individual coefficients a_i are complicated functions of the non-dimensional parameters, and provide little insight. Unlike Equation (1), this equation contains all powers of w up to three. However, the coefficient of the quadratic term, a_2, is linear in the electric field E_{x0}, and we take advantage of the arbitrariness of the frame of reference by choosing E_{x0} so that $a_2 = 0$. The specific expression for E_{x0} is complicated, and is not given here. (The stability properties of the system are independent of the choice of reference frame, i.e., of E_{x0}, as will be demonstrated.) Then dividing by the coefficient of the cubic term, the equation is of the form[1]

$$w^3 + a_1' w + a_0' = 0 \ , \tag{37}$$

which is now in the same form as Equation (1). The new coefficients a_i' are still complicated, and depend on specific assumptions, such as the presence, absence, or completeness of the FLR cancellations discussed in Section 1.2.

Equations of the form

$$x^3 - 3Ax + B = 0 \tag{38}$$

are called *deficient cubics* because of the absence of the quadratic term. They can be solved by using the substitution $x = \sqrt{A}(z + 1/z)$, which transforms Equation

---

[1]The general cubic can always be reduced to this form by means of the substitution $w = (z - a_2)/a_3$, see Ref. [7], Chapter 5.

(38) into a quadratic equation for z^3 whose roots are[2]

$$z_l = \left(-\frac{B}{2A^{3/2}} + \sqrt{\frac{B^2}{4A^3} - 1} \right)^{1/3} e^{2\pi i l/3}, \; l = 0, 1, 2 \; . \tag{39}$$

When $B^2/4A^3 < 1$, the values of z lie on the unit circle, so that $z^* = 1/z$, x is real, and the solutions are stable. When $B^2/4A^3 > 1$, the values of z do not lie on the unit circle, one root is real and two are complex conjugates. The root $l = 2$ has a negative imaginary part[3] which indicates instability.

Specific cases are considered below.

2.1.2   Complete FLR Cancellations

We now assume, as in most previous analyses, that both the gyro-viscous cancellation and the diamagnetic heat cancellation are complete. In this case, this assumption is exact for the diamagnetic heat flux but only approximate for the gyro-viscosity. The coefficients of Equation (37) remain complicated, but to lowest order in the small parameter δ_i, the dispersion relation reduces to

$$w^3 - \frac{1}{2}\alpha_z^2 \left(\beta_e + \frac{5}{3}\beta_i \right) w - \frac{1}{4}\alpha_y \alpha_z^2 \beta_i \beta_e \delta_i \eta_i = 0 \; , \tag{40}$$

which is just the non-dimensional form of the standard result, Equation (1). The "full" cubic contains terms that higher order in $k_\perp \rho_i \equiv \sqrt{\beta_i}\alpha_y \delta_i$. Equation (40) has the property that its solutions are stable when either $\beta_e = 0$ or $\beta_i = 0$.

The balance of the first two terns in Equation (40) give parallel sound waves,

$$w^2 = \frac{1}{2} \left(\beta_e + \frac{5}{3}\beta_i \right) \alpha_z^2 \; , \tag{41}$$

while the balance of the second (linear) and third (constant) terms yields a low frequency drift-like wave,

$$w = -2\beta_i \left(1 + \frac{1}{6}\beta_i \right) \eta_i \delta_i \alpha_y \; , \tag{42}$$

that propagates in the perpendicular (drift) direction. Instability results when the cubic term is balanced by the constant term.

---

[2]While the cubic has three solutions, the sixth order equation has six solutions. However, three of them are duplicates[7], and the cubic has only three unique roots.

[3]Recall that we use time dependence of e^{iwt}.

We have seen that the condition $B^2/4A^3 > 1$ is necessary for instability, where A and B are the coefficients appearing in Equation (38). Applying this to Equation (40), the instability condition is

$$\frac{27}{8} \frac{\alpha_y^2 \beta_i^2 \beta_e^2 \delta_i^2 \eta_i^2}{\alpha_z^2 \left(\beta_e + \frac{5}{3}\beta_i \right)^3} > 1 \ . \tag{43}$$

The system will become unstable when $\eta_i > \eta_i^{crit}$, where

$$\eta_i^{crit} = \left(\frac{2}{3} \right)^{3/2} \frac{\alpha_z}{\alpha_y} \frac{\left(\beta_e + \frac{5}{3}\beta_i \right)^{3/2}}{\beta_i \beta_e \delta_i} \ . \tag{44}$$

The condition for instability can also be written as $k_\perp \rho_i > g(\beta_i, \beta_e) k_z L_{Ti0}$. There is a threshold in $k_\perp \rho_i$ for the onset of instability, and instability is facilitated by long parallel wavelength ($\alpha_z/\alpha_y << 1$).

In deriving Equation (40), we chose the constant electric field E_{x0} so that the coefficient of the quadratic term vanished, leading to a deficient cubic. If instead we do not specify E_{x0}, but leave it arbitrary, then to lowest order in ϵ and δ_i we obtain[4]

$$w_E^3 - \frac{1}{2}\alpha_z^2 \left(\beta_e + \frac{5}{3}\beta_i \right) w_E - \frac{1}{4}\alpha_y \alpha_z^2 \beta_i \beta_e \delta_i \eta_i = 0 \ , \tag{45}$$

where $w_E = w - \alpha_y \delta_i \mathcal{E}_{x0}$. (Setting $w_E = 0$ is the same as Equation (35).) This is identical to Equation (40), so the stability properties of the system are independent of E_{x0}, as claimed previously[5]. The electric field produces a Doppler shifted frequency because it is equivalent to a coordinate transformation.

The first two terms in Equation (40) (or Equation (45)) produce a parallel sound wave. The constant term, which is responsible for the instability, has its origin in the term $\mathbf{V}_i \cdot \nabla p_{i0}$ in the ion energy equation. This describes advection of the equilibrium pressure by the perturbed ion flow ($V_{xi} dp_{i0}/dx \sim \eta_i$). It is abetted by the z-component of the electron momentum equation (parallel Ohm's law), which leads to a Boltzmann distribution of electron pressure and electrostatic potential along the magnetic field if $\beta_e > 0$. This couples the electron and ion dynamics. These effects can conspire to be in phase with, and reinforce, the pressure perturbations of the sound wave. If dp_{i0}/dx (i.e., η_i) is large enough, and $\beta_e > 0$, this can lead to instability.

---

[4]The equation is actually a full cubic, but the coefficient of the quadratic term is $O(\delta_i^3)$.

[5]This is expected, as the extended MHD equations, which are mathematically equivalent to the two-fluid equations, are independent of $\mathbf{E}_0$, but it is good to show it.

2.1.3 Incomplete Gyro-viscous Cancellation

We now consider the case when the gyro-viscous cancellation in the ion momentum equation is incomplete, but the diamagnetic heat cancellation remains complete. This is the most "physically realistic" case for the unsheared slab geometry under consideration. To lowest order in ϵ and δ_i, the dispersion relation is

$$w^3 - \frac{1}{2}\alpha_z^2\left(\beta_e + \frac{5}{3}\beta_i\right)w - \frac{1}{4}\alpha_y\alpha_z^2\beta_i\left[\beta_e\left(1 + \frac{1}{6}\beta_i\right) + \frac{5}{18}\beta_i^2\right]\delta_i\eta_i = 0 \ , \qquad (46)$$

This apparently allows the possibility of instability when $\beta_e = 0$. However, in that case the constant term is $O(\beta_i^3) << 1$ for $\beta_i < 1$. The critical value of η_i for the onset of instability is

$$\eta_i^{crit} = \left(\frac{2}{3}\right)^{3/2}\frac{\alpha_z}{\alpha_y}\frac{\left(\beta_e + \frac{5}{3}\beta_i\right)^{3/2}}{\beta_i\left[\beta_e\left(1 + \frac{1}{6}\beta_i\right) + \frac{5}{18}\beta_i^2\right]\delta_i} \ . \qquad (47)$$

This differs from Equation (44) by the factor in brackets in the denominator, which is $\sim \beta_e$ when $\beta_i << 1$. While this allows the possibility of instability when $\beta_e = 0$, it requires $\eta_i^{crit} \sim 1/\beta_i^3 >> 1$. When $\beta_e > 0$, Equation (47) agrees very well with Equation (44).

2.1.4 Incomplete Gyro-viscous Cancellation, No Diamagnetic Heat Flux

The goal of the present work is to verify the numerical solution of the two-fluid model in NIMROD by comparison with analytical solutions of the same equations under the same conditions. At the present time, the implementation of the ion diamagnetic heat flux in the NIMROD code has not been fully tested and debugged. Therefore, for comparison with numerical calculations, we consider the analytical solution of the two-fluid model with incomplete gyro-viscous cancellation and no diamagnetic heat flux. In this case, the dispersion relation to lowest order in ϵ and δ_i is

$$w^3 - \frac{1}{2}\alpha_z^2\left(\beta_e + \frac{5}{3}\beta_i\right)w - \frac{1}{4}\alpha_y\alpha_z^2\beta_i\left(\beta_e + \frac{5}{3}\beta_i\right)\left(1 + \frac{1}{6}\beta_i\right)\delta_i\eta_i = 0 \ . \qquad (48)$$

There is clearly the possibility of instability when $\beta_e = 0$, for then the constant term is $O(\beta_i^2) >> O(\beta_i^3)$. The value of η_i^{crit} is

$$\eta_i^{crit} = 2\sqrt{2}\frac{\alpha_z}{\alpha_z}\frac{\left(\beta_e + \frac{5}{3}\beta_i\right)^{1/2}}{\beta_i\left(1 + \frac{1}{6}\beta_i\right)\delta_i} \ , \qquad (49)$$

which is minimum when $\beta_e = 0$. The properties of the system without diamagnetic heat flux are both quantitatively and qualitatively different then the properties when it is included.

2.1.5   No Gyro-viscosity, No Diamagnetic Heat Flux

For completeness, we also consider the case with neither gyro-viscosity nor dia-magnetic heat flux. This corresponds to the Hall MHD model; it contains two-fluid effects but no FLR effects. The dispersion relation is a quadratic, whose solution at lowest order in ϵ and δ_i is

$$w^2 = \frac{1}{2}\alpha_z^2 \left(\beta_e + \frac{5}{3}\beta_i\right)\left[1 + \frac{3}{2}\alpha_y^2 \left(\beta_e + \frac{5}{3}\beta_i\right)\delta_i^2\right] \; . \tag{50}$$

This is a stable parallel sound wave with two-fluid corrections at second order in δ_i. For the ITG-like mode, gyro-viscosity is *destabilizing*.

2.1.6   Properties of the Solutions

Here we discuss the similarities and differences between the the solutions of the three dispersion relations derived in Sections 2.1.2, 2.1.3, and 2.1.4. We use the specific parameters $B_0 = 2$ T, $n_0 = 2 \times 10^{20}$ / m^3, $a = 1$ meter, $\alpha_y = 125.6$, and $\alpha_z = 0.1$ These result in $\delta_i = 0.0161$ and satisfy the ballooning ordering discussed in Section 1.1.

We first consider the values of η_i^{crit} given in Equations (44), (47) and (49). These are plotted in Figure 1 as functions of the electron temperature fraction $f_e = \beta_e/(\beta_i + \beta_e)$ for the case $\beta = \beta_i + \beta_e = 0.05$. The blue curve (Curve 1) is Equation (44) (diamagnetic heat flux and complete gyro-viscous cancellation), the red curve (Curve 2) is Equation (47) (diamagnetic heat flux and incomplete gyro-viscous cancellation), and the gold curve (Curve 3) is Equation (49) (no diamagnetic heat flux and incomplete gyro-viscous cancellation). Curve 1 is infinite at $f_e = 0$, indicating complete stability when $\beta_e = 0$. Curve 2 is finite but large ($\eta_i^{crit} = 18.6$) in this limit, so that instability when $\beta_e = 0$ is possible but the threshold is large. (Recall that Curve 2 represents the most "physically realistic" case.) All three curves are infinite when $f_e = 1$ ($\beta_i = 0$) indicating stability when the ions are cold. Curves 1 and 2 are in agreement when $f_e > 0$. For these parameters, instability is most easily achieved when $f_e \sim 0.7$, or $T_{e0}/T_{i0} \sim 7/3$. The gyro-viscous cancellation is apparently an excellent approximation. Curve 3 (no diamagtnetic heat flux) has completely different behavior: it is most unstable when $f_e = 0$ ($\beta_e = 0$), and is not even qualitatively similar to Curves 1 and 2 when $\beta_e > 0$. Clearly, the diamagnetic heat flux plays a crucial role in determining the stability of the system.

In Section 2.1.1 we showed that the solution of the cubic dispersion relation $w^3 - 3Aw + B = 0$ is $w = \sqrt{A}(z + 1/z)$, where z is given by Equation (39). Both the growth rate of the instability and its real frequency can be written explicitly in terms of the coefficients for each of the dispersion relations (40), (46), and (48), but
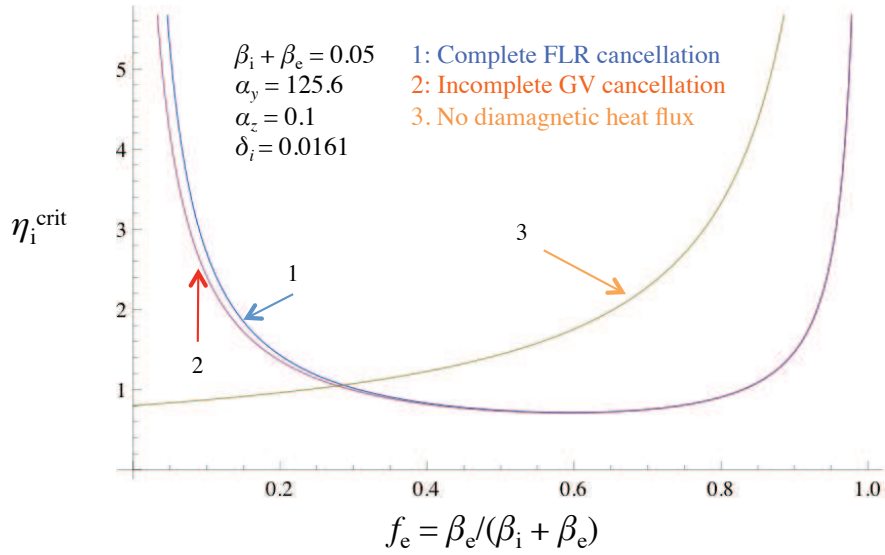
Figure 1: The instability criterion η_i^{crit} as a function of the electron β fraction for $\beta = \beta_e + \beta_i = 0.05$, $\alpha_y = 125.6$, $\alpha_z = 0.01$ and $\delta_i = 0.0161$. The blue curve assumes complete FLR cancellation (Section 2.1.2, Equation (44)); the red curve has incomplete gyro-viscous cancellation and complete diamagnetic heat cancellation (Section 2.1.3, Equation (47)); and, the gold curve has incomplete gyro-viscous cancellation and no diamagnetic heat flux (Section 2.1.4, Equation (49)). Curve 3 (gold) differs significantly from Curves 1 and 2, which are in good agreement.

the expressions are complicated and again yield little insight. Instead, we consider the behavior of the growth rate as a function of η_i for the specific parameters of Figure 1, and for different values of the electron β fraction f_e. This is shown in Figure 2a-d where we plot the growth rate $\gamma = -Im(w)$ as a function of η_i for four different values of $f_e = \beta_e/(\beta_i + \beta_e)$. Except for the monotonic behavior, there is little similarity between Curves 1 and 2, and Curve 3.

The behavior of the roots of the dispersion relation for the "most realistic" case of Section 2.1.3 is illustrated in Figure 3. The blue curve is the locus of the roots of Equation (46) in the (η_i, w) plane for the case $\beta_i = 0.01$, $\beta_e = 0.04$ ($T_{e0}/T_{i0} = 4$), and the remaining parameters of this Section. Also shown for comparison is the Doppler shifted zero frequency mode, Equation (35) (with $\mathcal{E}_{x0} = -\beta_i^2\eta_i/12$, as results at lowest order from reducing the dispersion relation to a deficient cubic), and the "low frequency wave"

$$ w = -\frac{1}{2}\alpha_y\beta_i\delta_i\eta_i\frac{\beta_e\left(1 + \frac{1}{6}\beta_i\right) + \frac{5}{18}\beta_i^2}{\beta_e + \frac{5}{3}\beta_i} \, , \tag{51} $$

which is obtained by equating the linear and constant terms in Equation (46). This
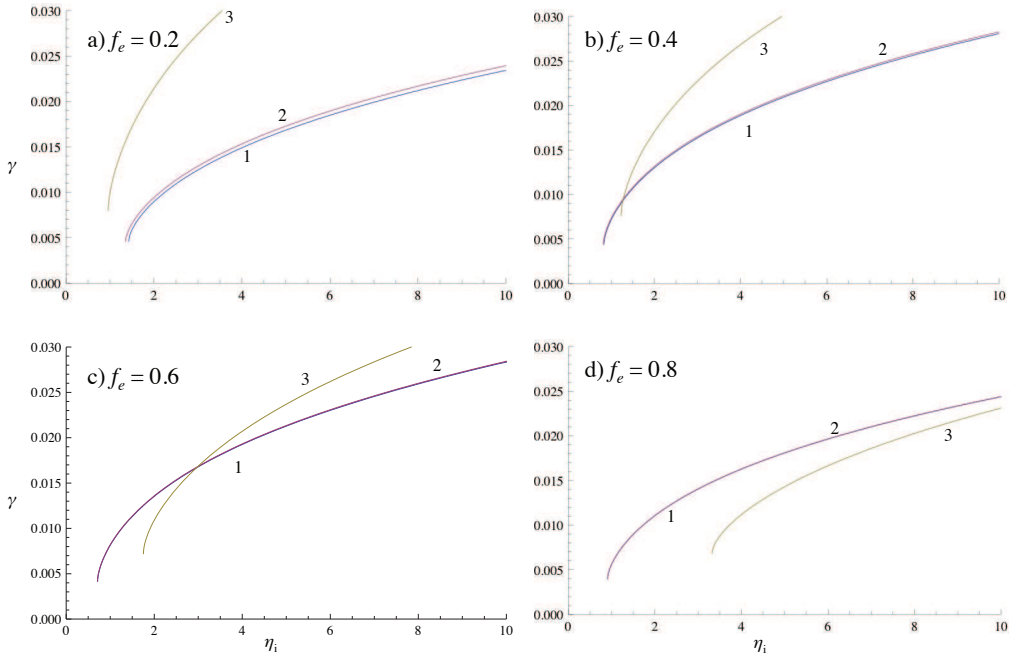

Figure 2: Growth rate of the electrostatic mode as a function of η_i for four different values of the electron β fraction: a) $f_e = 0.2$, b) $f_e = 0.4$. c) $f_e = 0.6$, and d) $f_e = 0.8$. In each case $\beta = \beta_i + \beta_e = 0.05$. The other parameters, and the labeling of the curves, is the same as in Figure 1. Curves 1 and 2 are almost identical except at low f_e.

has the appearance of a drift wave, but with a correction depending on β_e and β_i. When the medium is uniform ($\eta_i = 0$) this mode has zero frequency, and there two stable sound waves propagating in the $\pm z$-directions (three real roots); these sound waves are indicated by the dots in the figure. When $-\eta_i^{crit} < \eta_i < \eta_i^{crit}$ (where η_i^{crit} is given by Equation (47)), there are three real roots: Equation (51), the low frequency drift-like mode, and the two sound waves modified by two-fluid and FLR effects. When $|\eta_i| > \eta_i^{crit}$ there is one real root and two complex conjugate roots, with the growth rate of the unstable mode given by Curve 2 in Figure 2d. It is tempting to interpret the onset of instability as an "interaction" between the sound wave and the drift-like wave when they have comparable frequency.
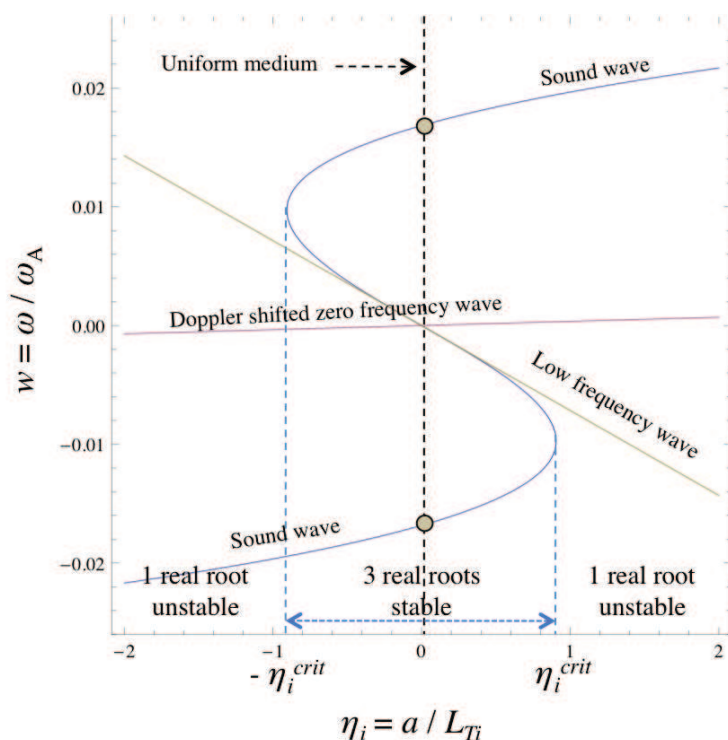
Figure 3: The locus of the roots of the dispersion relation with incomplete gyro-viscous cancellation and diamagnetic heat flux (Section 2.1.3) in the (η_i, w) plane for $\beta_i = 0.01$, $\beta_e = 0.04$ ($T_{e0}/T_{i0} = 4$), and the parameters of Figure 2. The red curve is the Doppler shifted zero frequency wave, Equation (35), the gold curve is the "low frequency" drift like wave, Equation (51), and the blue curve is the cubic dispersion relation, Equation (46). This cubic is has three real roots and is stable in the range $-\eta_i^{crit} < \eta_i < \eta_i^{crit}$; outside this range there is one real root and two complex conjugate roots, one if which is unstable with growth rate given in Figure 2d. The dots are the sound waves in a uniform medium.

17

2.2 Electromagnetic Modes

We now consider electromagnetic modes, so that $\mathbf{E} = -\nabla\phi - \partial\mathbf{A}/\partial t$. Here we work in a reference frame in which the ions are stationary at $x = 0$, so that $E_{x0} = \beta_i\delta_i\eta_i/2$. (Of course, the electrons drift in the opposite directon.) The solvability equation has two large roots, $\omega^2 >> \omega_A^2$, which we take as unphysical. The low order (in ϵ) solvability condition $F_0(w) = 0$ is sixth order, and factors as

$$(w - \frac{1}{2}\alpha_y\beta_i\delta_i\eta_i)f_5(w) = 0 \ . \tag{52}$$

The first factor appears as an ion drift wave, but is identical to the Doppler shifted zero frequency wave discussed in Section 2.1.1. The second is a quintic equation which has five roots: two shear Alfvén waves, two sound waves, and a low frequency waves similar to Equation (51).

The nature of the roots of the low order dispersion relation $f_5(w) = 0$ are illustrated[6] in Figure 5, including gyro-viscosity, diamagnetic heat flux, $\Gamma_e = 1$, and n_0 =constant, for the parameters of Section 2.1. The low frequency roots, including the drift wave (which in electrostatics appeared as the zero-frequency wave) have similar qualitative behavior to the electrostatic case, although the cubic behavior does not factor out of the quintic. The upper and lower branches are modified sound and magneto-acoustic waves. The remaining root is similar to the low frequency root given in Equation (51). The system is unstable when $|\eta_i| > \eta_{crit}$.

The electomagnetic mode is stable when $\beta_e \sim 0$. This is illustrated in Figure 5, where we plot the locus of the roots of the $f_5(w) = 0$ in the (f_e, w) plane for the parameters indicated in the figure, where $f_e = \beta_e/(\beta_i + \beta_e)$. There are five real roots when $f_e \to 0$ and $f_e \to 1$. There is an unstable root when $0.225 < f_e < 0.875$. The nature of the waves is indicated in the figure.

A comparison of the growth rate as a function of η_i for the electromagnetic (blue) and electrostatic (red) cases is shown in Figure 6. They are almost identical; the fluid ITG-like mode is essentially an electrostatic mode.

3 Computational Results

The computational algorithm for solving the extended MHD equations has been described in detail elsewhere[17]. The algorithm used here has $\kappa_i^{gv} = \kappa_e^{gv} = 0$, and assumes $\Gamma_e = 5/3$, but solves separate energy equations for the ions and electrons. The full gyro-viscous stress tensor is implemented. It therefore corresponds with

---

[6]Equations of degree 5 or higher do not have solutions that can be expressed in terms of radicals [7].
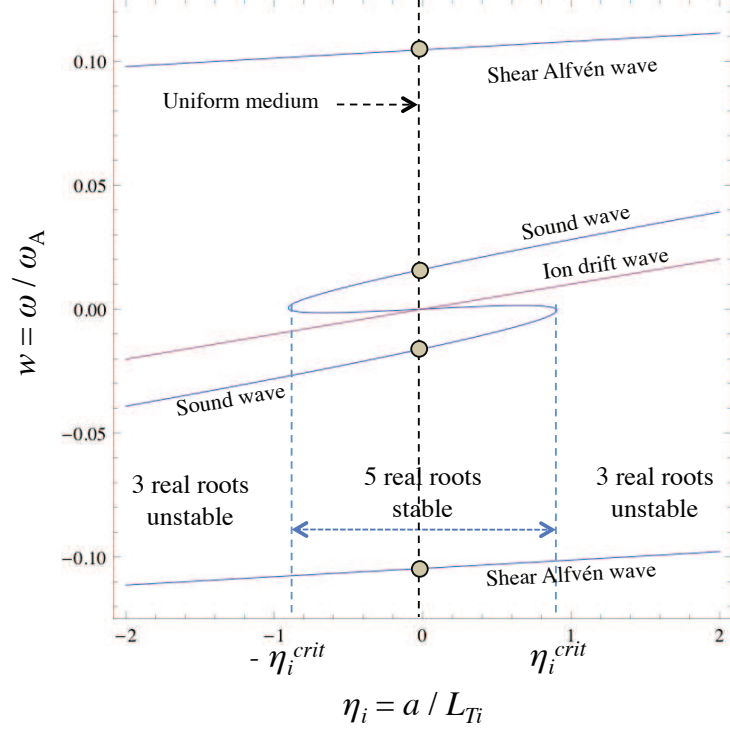
Figure 4: The locus of the roots of the electromagnetic dispersion relation with incomplete gyro-viscous cancellation and diamagnetic heat flux (Section 2.1.3) in the (η_i, w) plane for $\beta_i = 0.01$, $\beta_e = 0.04$ $(T_{e0}/T_{i0} = 4)$, and the parameters of Figure 2. The red curve is the ion drift wave. The blue curve is the quintic dispersion relation, $f_5(w) = 0$. The quintic is has five real roots and is stable in the range $-\eta_i^{crit} < \eta_i < \eta_i^{crit}$; outside this range there are three real roots and two complex conjugate roots, one if which is unstable. The low frequency behavior is similar to the electrostatic case; however, the cubic dies not factor out algebraically. The dots are the Alfvén and sound waves in a uniform medium.
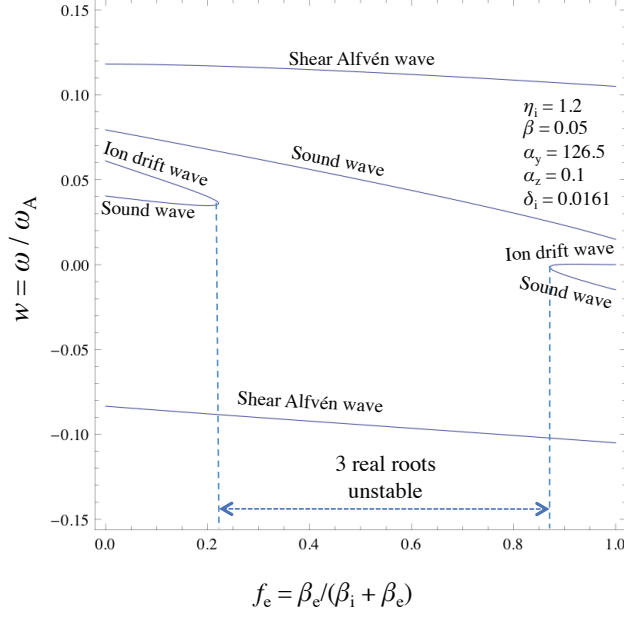
Figure 5: The roots of $f_5(w) = 0$ in the (f_e, w) plane, where $f_e = \beta_e/(\beta_i + \beta_e)$, for the parameters listed in the figure. The system is stable when $f_e \sim 0$ and $f_e \sim 1$.
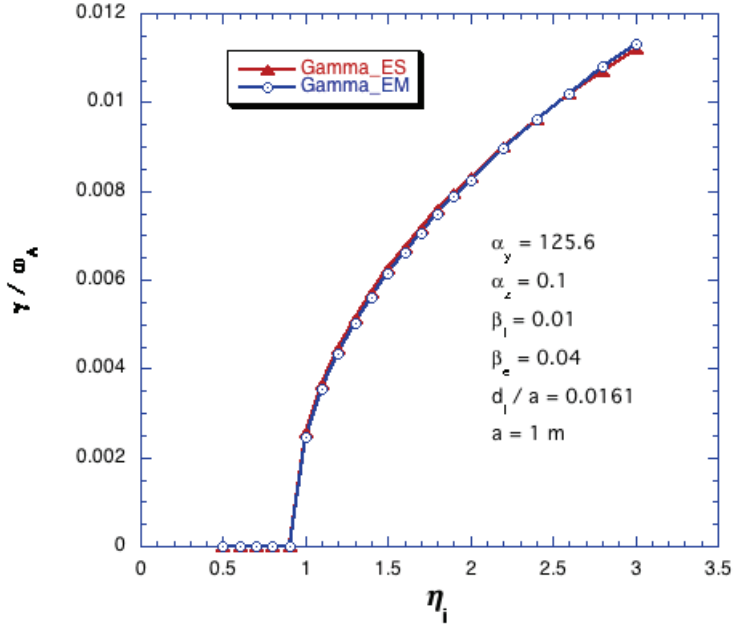

Figure 6: Comparison of the growth rate versus η_i for the electromagnetic (blue) and electrostatic (red) cases for n_0 =constant, $\Gamma_e = 1$, incomplete gyro-viscous cancellation, and diamagnetic heat flux.

the analytic results of Section 2.1.4 (but with $\Gamma_e = 5/3$), and should not be expected to agree with more the physically realistic models that include diamagnetic heat flux, especially when $\beta_e \to 0$. We can seek verification, but further code development is required for validation.

The linearized extended MHD equations are solved as an initial value problem using the equilibrium described in Section 2. Perfectly conducting, impermeable walls are placed at $x_{wall} = \pm 1$ meter; this serves as the distance normalization a used in the analytical results of Section 2: $n_0 = 10^{20}/\text{m}^3$, $B_0 = 2$ T, $\beta_i = 0.01$, and $\beta_e = 0.04$. We take n_0 =constant and T_{e0} =constant. The ion temperature varies as $T_{i0} = T_{i0}(0)e^{x/L_{Ti}}$, and define $\eta_i \equiv a/L_{Ti}$. We use the parameters of Section 2. These lead to $T_{e0} = 1.9$ KeV, $T_{i0}(0) = 0.5$ KeV, $V_A \equiv B_0/\sqrt{\mu_0 m_p n_0} = 3.08 \times 10^6$ m/sec, where m_p is the proton mass (a hydrogen plasma), and $d_i \equiv c/\omega_{pi} = 0.0161$ m.

The equilibrium is then perturbed with disturbances of the form $f(x, y, z, t) = \hat{f}(x, y, t)e^{ik_z z}$. The equations are solved on an (x, y) finite element grid, with periodic boundary conditions in y; the z-direction is assumed periodic and approximated by finite Fourier transforms. The parallel wave number k_z is a specified parameter, while the perpendicular wave number is $k_y = 2\pi/(y_{max} - y_{min})$. We choose $k_z = 0.1/\text{m}$ and $y_{max} = 0.025$ m, so that the non-dimensional wave numbers are $\alpha_z \equiv k_z a = 0.1$ and $\alpha_y \equiv k_y a = 126.5$. The linearized extended MHD equations are then integrated forward in time. The fastest exponentially growing solution (if there is one) will emerge from the initial perturbations as $t \to \infty$.

The computational algorithm solves the differential equations of the extended MHD model including full x-dependence of the perturbations, and imposes boundary conditions at $x = \pm x_{wall}$. Neither of these are included in the analysis of Section 2; the local approximation is not assumed, and the solutions may have rapid x-variation. Since the fundamental algorithm has very low inherent numerical dissipation[8, 17], we have found it necessary to introduce a small amount of dissipation in the form of electrical resistivity, viscosity, and isotropic thermal conductivity. The particular values correspond to a Lundquist number $S = 10^9$, magnetic Prandtl number $P_{rM} = 1$. We have also found it useful to increase the resistivity and viscosity by a factor of 10^2 is a small layer near $\pm x_{wall}$. A small amount of hyper-diffusivity is used in the continuity equation: $D_{nh} = 10^{-2}$ m^4/sec. The boundary conditions at $\pm x_{wall}$ are: no-slip ($\mathbf{V} = 0$), $B_n = 0$, $E_{tan} = 0$, and Dirichlet conditions (fixed values) for density and temperature. We make a series of runs and keep all parameters fixed except L_{Ti}. The results are converged in time and spatial resolution, and dissipation. If there is an unstable mode, we determine its growth rate γ as a function of $\eta_i \equiv a/L_{Ti}$.

For the given parameters, the computational algorithm finds an unstable mode with threshold $\eta_i^{crit} \sim 0.7$. These results are shown in Figure 7, where we plot

the growth rate of the unstable mode (in units of sec^{-1}) determined numerically is plotted as a function of η_i for the given parameters. For comparison, we also plot the predictions of the local electromagnetic theory described in Section 2.1.4, evaluated with the parameters at $x = 0$, using $\Gamma_e = 5/3$, and $\kappa_i^{gv} = \kappa_e^{gv} = 0$ (as in the numerical calculations). While there is fair agreement on the marginal point η_i^{crit}, NIMROD predicts consistently larger growth rates than the local theory.
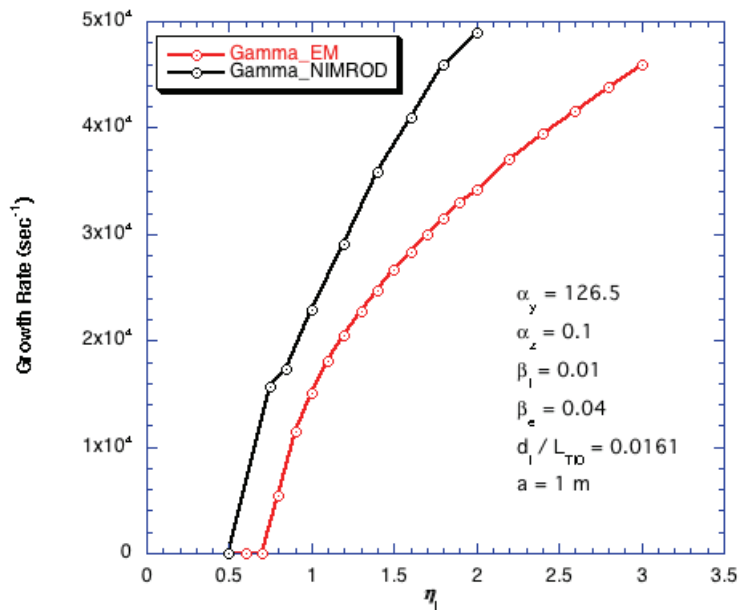
Figure 7: Growth rate of the unstable mode determined by numerically (NIMROD) compared with the predictions of the local theory for the given parameters. Both results take $\Gamma_e = 5/3$ and $\kappa_i^{gv} = \kappa_e^{gv} = 0$.
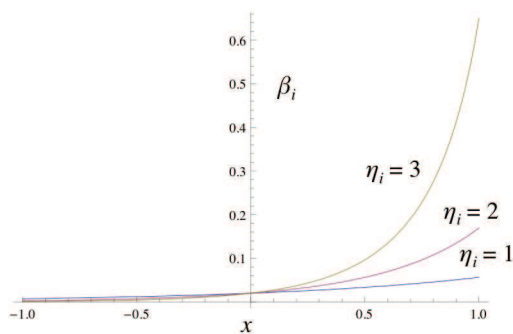

Figure 8: Variation of β_i as a function of x for the equilibrium $T_{i0}(x) = e^{\eta_i x}$, $n_0 = $ constant, and $\beta_i(0) = 0.02$, for three different values of η_i.

22

In addition to the fixed parameters $\alpha_y, \alpha_z, \eta_i, \delta_i$ and β_e, the theoretical growth rate depends on the local value of β_i, and the normalization on the local value of $\omega_A = V_A/a$. We emphasize that the analytic results plotted in Figure 7 were obtained using parameters evaluated at $x = 0$. In fact, these parameters depend on x: $\beta_i(x) = \beta_i(0)p_{i0}(x)/B_{0z}(x)^2$, and $\omega_A(x) = B_{0z}(x)/(a\sqrt{n_0})$. The variation of $\beta_i(x)$ for $\eta_i = 1, 2$, and 3 is shown in Figure 8. (The parameters β_e and $\delta_i = d_i/a$ are constant if the density and electron temperature are constants.) Because of the exponential nature of the equilibrium, regions near the outer boundary ($x = 1$) can have $\beta_i \sim 1$ even for moderate η_i.

As a result of this variation, the local theory developed in Section 2 predicts a different local growth rate at each value of x. In contrast, the numerical algorithm produces a single global eigenmode that varies with x and has a single growth rate. These points are illustrated in Figure 9, where the local growth rate is plotted as a function of η_i for different locations x of the equilibrium profile. The growth rate of the global mode is also shown as a function of η_i. (These are the same data plotted in Figure 7.) The connection between the single global growth rate and the individual local growth rates is not obvious.

The structure of the global eigenfunction of the perturbed ion temperature is shown in Figure 10 for a)$\eta_i = 0.75$, b) $\eta_i = 1.0$, c)$\eta_i = 1.4$ and d) $\eta_i = 1.8$. The striated appearance is due to the shear in the drift velocity $V_{iy0}(x)$; see Equation
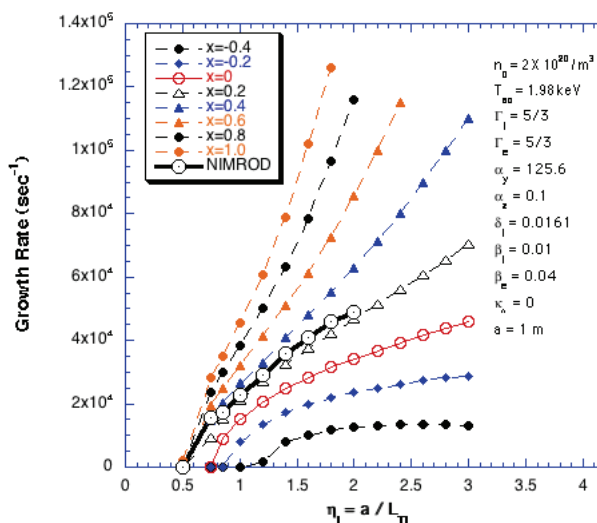

Figure 9: The local growth rate as a function of η_i for different values of x. The computational results for the growth rate of the global eigenfunction are labeled NIMROD. This case has an exponential ion temperature profile, $\alpha_y = 125.6$, $\alpha_z = 0.1$, $\beta_i = 0.01$, $\beta_e = 0.04$, and $\delta_i = 0.0161$.

(29). These structures correspond to counter-rotating vortices. The eigenfunction migrates toward the upper (high β) boundary as η_i increases.

The global eigenfunctions displayed in Figure 10a), b), and c) appear to be time asymptotic states; they maintain the same spatial structure and continue to grow exponentially for as long as the time-dependent calculation is continued. However, the mode for $\eta_i = 1.8$, Figure 10d), eventually undergoes a transition to a faster
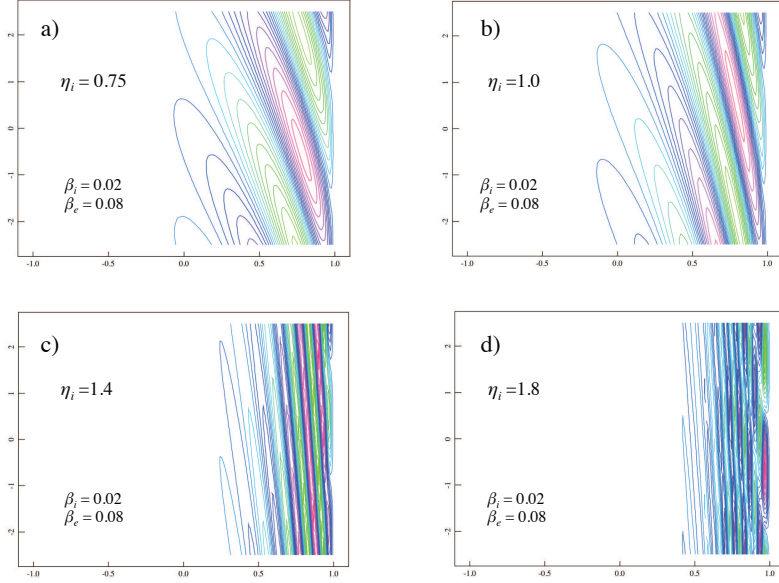

Figure 10: The spatial structure of the global ITG eigenfunction for a) $\eta_i = 0.75$, b) $\eta_i = 1.0$, c) $\eta_i = 1.4$, and d) $\eta_i = 1.8$, for the exponential case with f $\alpha_y = 125.6$, $\alpha_z = 0.1$, $\beta_i = 0.01$, $\beta_e = 0.04$, and $\delta_i = 0.0161$. The eigenfunction migrates toward the upper (high β) boundary as η_i is increased.
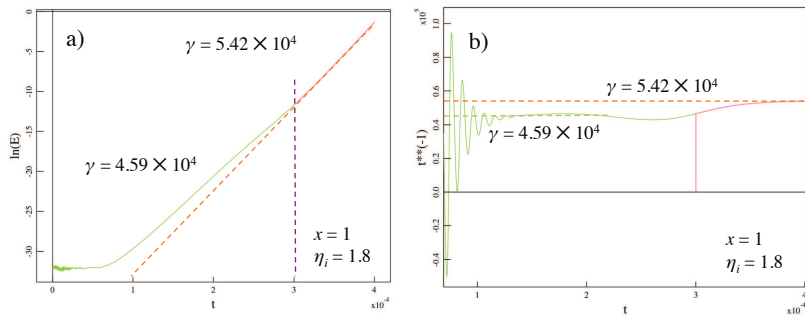

Figure 11: a) The log of the energy of the unstable mode as a function of time for the low β parameters at $x = 1$. The slope ($\sim \gamma$) increase at $t \sim 3 \times 10^{-4}$ seconds. b) The growth rate $\gamma = (1/2)d(\ln E)dt$ corresponding to part a).

growing mode at large time. This is illustrated in Figure 11a), where we plot the logarithm of the energy in the unstable mode as a function of time. The slope increases at $t \sim 3 \times 10^{-4}$ seconds, but the mode continues to grow exponentially. The growth rate of the modes is $\gamma = (1/2)d(\ln E)dt$. In Figure 11b) we plot γ as a function of time for this case. After settling into nearly exponential growth at $t \sim 1 \times 10^{-4}$ seconds, it makes a transition to a larger value at $t \sim 3 \times 10^{-4}$ seconds, and then continues at this value.

The eigenfunction for $t > 3 \times 10^{-4}$ seconds is shown in Figure 12. It is concentrated near $x = 1$. In spite of its pathological appearance, it appears to be well resolved numerically.

In Section 2.1.4 we noted that the two-fluid model with gyro-viscosity but no diamagnetic heat flux indicates that ITG-like electrostatic modes are unstable when $\beta_e = 0$. At the present time, the implementation of the diamagnetic heat flux in NIMROD is still being tested and debugged. Therefore, the NIMROD results should be compared with the theory of Section 2.1.4. In Figure 13 we plot the growth rate as a function of the electron temperature fraction $f_e = \beta_e/(\beta_e + \beta_i)$ for fixed $\beta = \beta_e + \beta_i = 0.05$ and $\eta_i = 1.2$. The other parameters are the same as used in Figure 9. The red curve is the solution of Equation (48); it is the lowest order (in ϵ and δ_i) electrostatic solution in the local approximation with gyro-viscosity but no diamagnetic heat flux. The blue curve is the full solution of
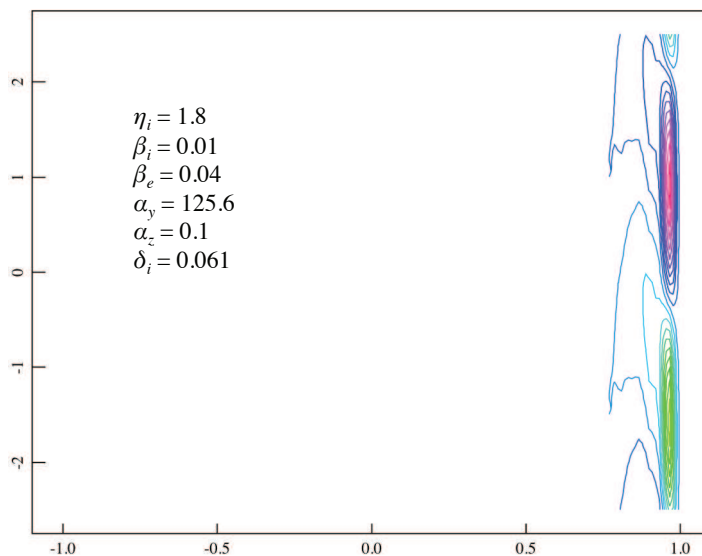

Figure 12: The spatial structure of the global eigenfunction for $\eta_i = 1.8$ for $t > 3 \times 10^{-4}$ seconds. In spite of its localization near $x = 1$, the mode appears to be well resolved numerically. It has a larger growth rate than the eigenmode shown in Figure 10.
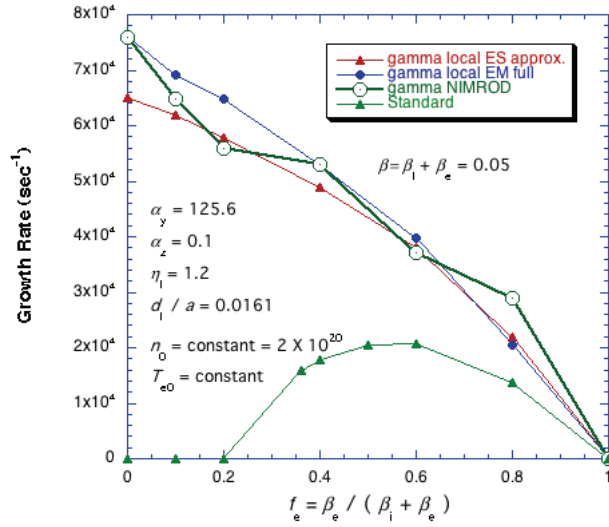
Figure 13: Growth rate as a function of the electron temperature fraction, $f_e = \beta_e/(\beta_i + \beta_e)$, for fixed $\beta = \beta_i + \beta_e = 0.05$ and $\eta_i = 1.2$. The other parameters are $alpha_y = 126.5$, $\alpha_z = 0.1$, and $\delta_i = 0.0161$. The red curve is the approximate local electrostatic solution determined with Equation (48). The blue curve is the electromagnetic solution using only the local approximation ($\epsilon = 1$) that satisfies the quintic equation $f_5(w) = 0$. The dark black curve is the numerical results from the NIMROD code. We also display for comparison the more accurate solution that contains diamatnetic heart flux, as given in Equation (40).

the electromagnetic dispersion relation $f_5(w) = 0$, using the local approximation but no further ordering ($\epsilon = 1$). The dark black curve is the numerical solution obtained with the NIMROD code. There is good agreement between these results. More striking is the disagreement between these solutions and the solution of Equation (40), which does not allow instability when $f_e = 0$. While there is good agreement between the analytic and computational results for the same parameters (i.e., no diamagnetic heat flux), both disagree with the more realistic models (with diamagnetic heat flux) across the entire range of β_e. The computational model is verified, but not validated. Clearly, the model of ion diamagnetic heat flux needs to be refined and tested in the NIMROD code.

4 Discussion

The dynamics of a magnetized plasma are described by the evolution of the distribution functions according to the plasma kinetic equation (PKE) for each species. This kinetic model contains a large number of degrees of freedom. These can be reduce by considering the evolution of the velocity moments of the distribution functions and the corresponding PKEs. The two-fluid model considers the dynamics only a few of these lowest order moments that introduce the lowest order corrections (in $k_\perp \rho_i$) to ideal MHD. Here we are concerned with how well the solutions of the two-fluid model correspond to the solutions of the underlying PKEs.

We have analyzed the stability of the two-fluid model for the case in Cartesian slab geometry where there is no shear in the magnetic field and the equilibrium density and electron temperature are spatially uniform, but there is a gradient in the equilibrium ion temperature. There can be instability if the temperature gradient is sufficiently large. This configuration is stable in ideal MHD; it is destabilized by effects of finite ion Larmor radius (FLR). It s therefore a good test case for judging the efficacy of using the two-fluid model for describing the dynamics of highly magnetized, hot, nearly collisionless plasmas.

The two-fluid model contains terms in the ion momentum and energy equations, the gyro-viscous stress and the ion diamagnetic heat flux, that together approximate the effects of finite ion Larmor radius on the global dynamics of the plasma. The terms enter the theory at the same order (in $k_\perp \rho_i$), and they should both be included for the model to be consistent[7]. Together, their effect is to almost completely cancel the contributions of advection by the ion diamagnetic drift velocity; see Section 1.2. If they are both excluded (so-called Hall MHD) the system has stable solutions; see Section 2.1.5. If only the gyro-viscosity is retained

---

[7]There is another term, the *diamagnetic heat stress*, that also enters the ion stress tensor [11]. However, it is one order higher in $k_\perp \rho_i << 1$ than the gyro-viscous stess and does not affect the results to lowest order.

the system is unstable, but the instability persists in the limit $\beta_e \to 0$; Section 2.1.4. When they are both retained, either exactly or approximately, the system is unstable, but is stable when $\beta_e \to 0$; Sections 2.1.2 and 2.1.3. This latter result is in agreement with the predictions of kinetic theory [2, 6].

The current version of the NIMROD code contains a complete implementation of the ion gyro-viscous stress, but the implementation of the diamagnetic heat flux is still undergoing testing and debugging. It is thus a numerical implementation of the model of Section 2.1.4: incomplete gyro-viscous cancellation and no diamagnetic heat flux. In this case, the computational solutions agree reasonably well with the local analytic solutions. In particular, they both predict instability when $\beta_e \to 0$, in disagreement with both kinetic theory and two-fluid theory that retains the diamagnetic heat flux. Therefore, the computational solutions of the two fluid equations are accurate, but the model is not correct (or, perhaps, is incomplete); NIMROD has been verified but not validated for this problem. Completion of the computational implementation of the diamagnetic heat flux in the NIMROD (and other) extended MHD codes is therefore necessary to obtain a physically realistic two-fluid model, and should be a development priority.

There is also a question of how well the full two-fluid model agrees with kinetic theory over a range of parameters, i.e., β_i, β_e, $k_\perp \rho_i$, etc. This can best be determined by running the same problem with a kinetic code (Lorentz ions, or possibly gyro-kinetic) and comparing with the two-fluid (extended MHD) results in detail.

Progress in extending fluid models further into the kinetic regime requires the implementation of more accurate (i.e., higher order in $k_\perp \rho_i$) closure schemes for the ion stress tensor and heat flux. (Implementing the diamagnetic heat stress into the ion dynamics has not been addressed, either.) The problem of ITG-like modes analyzed here is a good test case of these models.

References

[1] L. I. Rudakov and R. Z. Segdeev, Soviet Phys. - Doklady **6**, 415 (1961).

[2] B. Coppi, M. N. Rosenbluth and R. Z. Segdeev, Phys. Fluids **10**, 582 (1967).

[3] C. C. Hegna, Lecture notes, undated, private communication (2011).

[4] C. R. Sovinec, private communication (2011).

[5] Jan Weiland, *Collective Modes in Inhomogeneous Plasma*, Institute of Physics Publishing, Bristol and Philadelphia, 2000.

[6] T. H. Stix, *Waves in Plasmas*, Second Edition, Problems 3.5, 14.6 and 14.7, AIP, 1992.

[7] F. Cajori, *An Introduction to the Theory of Equations*. Dover, New York, 1969.

[8] NIMROD Ref.

[9] M3D-C1 Ref.

[10] Schnack, APS tutorial paper, Phys. Plasmas

[11] R. D. Hazeltine and J. D. Meiss, *Plasma Confinement*, pp. 208ff, Addison-Wessley, Redwood City, 1992.

[12] P. N. Guzdar, L. Chen, W. M. Tang and P. H. Rutherford, Phys. Fluids **26**, 673 (1983)

[13] S. C. Guo and J. Weiland, Nucl. Fusion **37**, 1095 (1997).

[14] G. W. Hammet and F. W. Perkins, Phys. Rev. Letter. **64**, 3019 (1990).

[15] S. E. Parker, W. Dorland, R. A. Santoro, M. A. Beer, Q. P. Liu, W. W. Lee and G. W. Hammet, Phys. Plasmas **1**, 1461 (1994).

[16] Mathematica Ref.

[17] C. R. Sovinec, J. R. King, and the NIMROD Team, J. Comput. Phyics **229**, 5803 (2010).

Appendix A: Linearized Two-fluid Equations

The non-dimensional linearized two-fluid equations are

$$\frac{\partial n}{\partial t} = -\nabla \cdot (n_0 \mathbf{V}_i + n \mathbf{V}_{i0}) \ , \tag{53}$$

$$\frac{\partial n}{\partial t} = -\nabla \cdot (n_0 \mathbf{V}_e + n \mathbf{V}_{e0}) \ , \tag{54}$$

$$\delta_i n_0 \left(\frac{\partial \mathbf{V}_i}{\partial t} + \mathbf{V}_{i0} \cdot \nabla \mathbf{V}_i + \mathbf{V}_i \cdot \nabla \mathbf{V}_{i0} \right) = n \left(\mathbf{E}_0 + \mathbf{V}_{i0} \times \mathbf{B}_0 \right)$$
$$+ n_0 \left(-\nabla \phi - \frac{\partial \mathbf{A}}{\partial t} + \mathbf{V}_i \times \mathbf{B}_0 + \mathbf{V}_{i0} \times \mathbf{B} \right) - \frac{1}{2} \beta_i \delta_i \left(\nabla p_i + \delta_i \nabla \cdot \mathbf{\Pi}_i^{gv} \right) \tag{55}$$

$$0 = -n \left(\mathbf{E}_0 + \mathbf{V}_{e0} \times \mathbf{B}_0 \right) - n_0 \left(-\nabla \phi - \frac{\partial \mathbf{A}}{\partial t} + \mathbf{V}_i \times \mathbf{B}_0 + \mathbf{V}_{i0} \times \mathbf{B} \right) - \frac{1}{2} \beta_e \delta_i \nabla p_e \ , \tag{56}$$

$$\frac{\partial p_i}{\partial t} + \mathbf{V}_{i0} \cdot \nabla p_i + \mathbf{V}_i \nabla p_{i0} = -\Gamma_i \left(p_{i0} \nabla \cdot \mathbf{V}_i + p_i \nabla \cdot \mathbf{V}_{i0} \right)$$
$$- (\Gamma_i - 1) \frac{1}{2} \beta_i \delta_i \nabla \cdot \mathbf{q}_{gv}^i, , \tag{57}$$

$$\frac{\partial p_e}{\partial t} + \mathbf{V}_{e0} \cdot \nabla p_e + \mathbf{V}_e \nabla p_{e0} = -\Gamma_e \left(p_{e0} \nabla \cdot \mathbf{V}_e + p_e \nabla \cdot \mathbf{V}_{e0} \right)$$
$$- (\Gamma_e - 1) \left(\nabla \cdot \mathbf{q}_u^e + \frac{1}{2} \beta_i \delta_i \nabla \cdot \mathbf{q}_{gv}^e \right), \tag{58}$$

$$\delta_i \nabla^2 \mathbf{A} = -n_0 \left(\mathbf{V}_i - \mathbf{V}_e \right) - n \left(\mathbf{V}_{i0} - \mathbf{V}_{e0} \right) \ , \tag{59}$$

and

$$\mathbf{B} = \nabla \times \mathbf{A} \ , \tag{60}$$

along with the condition $\nabla \cdot \mathbf{A} = 0$.

The linearized gyro-viscous stress is

$$\mathbf{\Pi}_i^{gv} = \frac{1}{2} \left[\eta_{30} \mathbf{F} \cdot \mathbf{W}(\mathbf{V}_i) + \eta_3 \mathbf{F} \cdot \mathbf{W}(\mathbf{V}_{i0}) \right] \ , \tag{61}$$

where $\eta_{30}(x) = p_{i0}(x)/B_0(x)$, and

$$\eta_3(x) = \frac{1}{B_0(x)} \left[p_i - \frac{p_{i0}(x)}{B_0(x)^2} B_z \right] \tag{62}$$

is the perturbed gyro-viscous coefficient. The linearized gyro-heat fluxes are

$$\mathbf{q}^s_{gv} = \pm \left[\kappa^s_{gv0} \hat{\mathbf{b}}_0 \times \nabla T_s + \kappa^s_{gv} \hat{\mathbf{b}}_0 \times \nabla T_{s0} + \kappa^s_{gv0} \hat{\mathbf{b}} \times \nabla T_{s0} \right] \ , \qquad (63)$$

where again $(+)$ refers to ions $(s = i)$, $(-)$ refers to electrons $(s = e)$, $\kappa^s_{gv0} = (5/2) p_{s0}(x)/B_0(x)$,

$$\kappa^s_{gv}(x) = \frac{5}{2} \frac{1}{B_0(x)} \left[p_s - \frac{p_{s0}(x)}{B_0(x)} B_z \right] \ , \qquad (64)$$

is the perturbed gyro-conductivity, $\hat{\mathbf{b}}_0 = \hat{\mathbf{e}}_z$, and

$$\hat{\mathbf{b}}(x) = \frac{1}{B_0(x)} \left(B_x \hat{\mathbf{e}}_x + B_y \hat{\mathbf{e}}_y + B_z \hat{\mathbf{e}}_z \right) \ , \qquad (65)$$

is the direction of the perturbed field. The perturbed temperature is $T_s = [p_s - n/n_0(x)]/n_0(x)$. Finally,

$$\mathbf{q}^e_u = 0.71 \left[p_e \hat{\mathbf{b}}_0 \cdot (\mathbf{V}_{e0} - \mathbf{V}_{i0}) + p_{e0} \hat{\mathbf{b}}_0 \cdot (\mathbf{V}_e - \mathbf{V}_i) + p_{e0} \hat{\mathbf{b}} \cdot (\mathbf{V}_{e0} - \mathbf{V}_{i0}) \right] \ . \qquad (66)$$

Since the the condition $\nabla \cdot \mathbf{A} = 0$ must be enforced, only two components of Ampére's law, Equation (59), are required.

Appendix B : Algebraic System of Equations

We display the individual equations of the algebraic system that are solved in Section 2. We have assumed $n_0 = 1$; when n_0 is not constant it appears explicitly in these equaitons, and the algebraic manipulations becomes more complicated.

The equations are: ion continuity,

$$wn + \alpha_y V_{yi} + \alpha_z V_{zi} = 0 , \tag{67}$$

electron continuity,

$$\left(w - \frac{1}{2}\alpha_y\beta_i\delta_i\eta_i \right) n + \alpha_y V_{ye} + \alpha_z V_{ze} = 0 , \tag{68}$$

ion x-momentum,

$$
\begin{aligned}
-\frac{1}{2}\beta_i\delta_i\eta_i n &+ i\delta_i\left[w - \frac{1}{4}\alpha_y\beta_i\left(1 + \frac{1}{2}\beta_i\right)\delta_i\eta_i \right]V_{xi} \\
&- \left[1 - \frac{1}{4}\beta_i\delta_i^2\left(\alpha_y^2 + 2\alpha_z^2\right) \right]V_{yi} + \frac{1}{2}\alpha_y\alpha_z\beta_i\delta_i^2 V_{zi} \\
-\frac{1}{3}\beta_i^2\left(1 + \frac{3}{2}\beta_i\right)\delta_i^3\beta_i^3 p_i &+ iwA_x + \frac{1}{4}\beta_i^2\left(1 + \beta_i\right)\delta_i^3\eta_i^3 B_z = 0,
\end{aligned}
\tag{69}
$$

ion y-momentum,

$$
\begin{aligned}
\left[1 - \frac{1}{4}\beta_i\delta_i^2\left(\alpha_y^2 + 2\alpha_z^2 - 2\eta_i^2\right) \right]V_{xi} \\
+ i\delta_i\left[w - \frac{1}{4}\alpha_y\beta_i\left(1 + \frac{1}{2}\beta_i\right)\delta_i\eta_i \right]V_{yi} \\
- i\alpha_y\phi + iwA_y - \frac{1}{8}i\alpha_y\beta_i^2\delta_i^2\eta_i^2 B_z = 0,
\end{aligned}
\tag{70}
$$

ion z-momentum,

$$
\begin{aligned}
-\frac{1}{2}\alpha_y\alpha_z\beta_i\delta_i^2 V_{xi} - \frac{1}{2}i\alpha_z\beta_i\left(1 + \frac{1}{2}\beta_i\right)\delta_i^2\eta_i V_{yi} \\
+ i\delta_i\left[w - \frac{1}{2}\alpha_y\beta_i\left(1 + \frac{1}{2}\beta_i\right)\delta_i\eta_i \right]V_{zi} \\
+ i\alpha_z\phi + \frac{1}{2}\alpha_z\beta_i\delta_i p_i + iwA_z = 0,
\end{aligned}
\tag{71}
$$

electron x-momentum,

$$V_{ye} - iwA_x - \frac{1}{2}\beta_i\delta_i\eta_i B_z = 0 , \tag{72}$$

electron y-momentum,

$$V_{xe} + i\alpha_y\phi - \frac{1}{2}i\alpha_y\beta_e\delta_i p_e + iwA_y = 0 \ , \tag{73}$$

electron z-momentum,

$$i\alpha_z\phi + \frac{1}{2}i\alpha_z\beta_e\delta_i p_e - iwA_z + \frac{1}{2}\beta_i\delta_i\eta_i B_x = 0 \ , \tag{74}$$

ion energy,

$$\frac{5}{3}i\alpha_y\beta_i\left(1 + \frac{1}{4}\beta_i\right)\delta_i\eta_i n + \eta_i V_{xi} + \frac{5}{3}i\alpha_y V_{yi} + \frac{5}{3}i\alpha_z V_{zi}$$
$$+i\left(w - \frac{5}{12}\alpha_y\beta_i^2\delta_i\eta_i\right)p_i - \frac{1}{3}i\alpha_z\beta_i\delta_i\eta_i B_y \quad = \quad 0, \tag{75}$$

electron energy,

$$\alpha_y V_{ye} + \alpha_z V_{ze} + \left(w - \frac{1}{2}\alpha_y\beta_i\delta_i\eta_i\right)p_e = 0 \ , \tag{76}$$

the x-component of Ampére's law,

$$V_{xi} - V_{xe} - \delta_i\left(\alpha_y^2 + \alpha_z^2\right)A_x = 0 \ , \tag{77}$$

the z-component of Ampére's law,

$$V_{zi} - V_{ze} - \delta_i\left(\alpha_y^2 + \alpha_z^2\right)A_z = 0 \ , \tag{78}$$

the gauge condition $\nabla \cdot \mathbf{A} = 0$,

$$\alpha_y A_y + \alpha_z A_z = 0 \ , \tag{79}$$

and the three components of $\mathbf{B} = \nabla \times \mathbf{A}$,

$$B_x + i\alpha_z A_y - i\alpha_y A_z = 0 \ , \tag{80}$$

$$B_y - i\alpha_z A_x = 0 \ , \tag{81}$$

and

$$B_z + i\alpha_y A_x = 0 \ . \tag{82}$$